Progress In Electromagnetics Research, PIER 41, 61–81, 2003

DISPERSION DIAGRAMS OF BLOCH MODES APPLIED TO THE DESIGN OF DIRECTIVE SOURCES

S. Enoch, G. Tayeb, and D. Maystre

Institut Fresnel, UMR 6133
Faculté des Sciences et Techniques de Saint-Jérôme
Case 16 1, 13397 Marseille Cedex 20, France

Abstract—We present an original study which makes use of a convenient representation of the dispersion diagrams of Bloch modes for the design of angular selective sources. These diagrams provide us all the pertinent information about the radiative properties of the photonic crystal, and a guideline to optimize the structure in order to obtain the suitable properties. We apply these tools in two cases: when the radiated field propagates normally to the device, and also for an off-axis radiating device. Several numerical examples obtained from a rigorous numerical method show the relevance of this approach.

1. INTRODUCTION

Photonic crystals have been extensively studied in the recent years, in the framework of microwave and optical applications. Several works have been aimed towards the improvement of the performances of antennas in the microwave range of frequencies. Among them, a

special attention has been paid to the use of the photonic crystals as plane reflecting devices for antennas, able to eliminate the well known drawbacks of a conducting ground plane. In that case, it has been demonstrated that the improvements come from a tunable phase shift for the reflected waves, and from the ability of this structure to prevent the propagation of surface waves [1–7]. A second direction of research deals with the use of resonant cavities (or defects in the photonic crystal) to reduce the angular range of the emitted field [8, 9].

In this paper, we propose an alternative way to enhance the directivity of an emitting device. It is based on the intrinsic properties of the photonic crystal material. The directional radiation is obtained using new kinds of photonic crystals used near the band-gap edge. It turns out that the adequate tool for describing this property is an original analysis based on a three-dimensional representation of the dispersion relations of the Bloch modes propagating inside the crystal. This approach is illustrated in the case of a two-dimensional dielectric structure. At a given frequency, a section of this three-dimensional graph gives a constant-frequency dispersion diagram, which allows us to predict both the energy flow inside the crystal, and the phase variations of the field. We show that if the structure is large enough in the transverse direction, the emitted field outside the crystal is radiated in a narrow angular range provided that this constant-frequency dispersion diagram responds to specific requirements.

This property is obtained on two examples by expanding the hexagonal lattice of the photonic crystal in a convenient direction. In the first one, the device radiates in the direction orthogonal to the mean surface of the device. In the second one, the light propagates in an arbitrarily chosen direction. In both cases, the structure is fed by a simple wire antenna, one of the interesting features of these devices being to allow the use of any localized light source inside the crystal.

2. DISPERSION DIAGRAMS

2.1. Energy and Phase Velocities

In this paper, we use a rectangular coordinate system (O, x, y, z). The unit vectors of the axes are $\mathbf{e}_x, \mathbf{e}_y$, and $\mathbf{e}_z$. Harmonic fields are expressed using a time dependence in $\exp(-i\omega t)$, with $\omega = 2\pi c/\lambda = ck_0$, c being the speed of light in vacuum, λ the wavelength and k_0 the wavenumber in vacuum.

We consider two-dimensional photonic crystals made with lossless materials (dielectric or perfectly conducting). The 2D photonic crystal is invariant by translation along the z-axis, and we consider

z-independent electromagnetic fields. Consequently, the problem reduces to two independent scalar problems, that we call $E\|$ or $H\|$ according to whether the electric or magnetic field is parallel to the z-axis. We denote by $u(x, y)$ the relevant component of the total field (E_z or H_z depending on the polarization case).

Let us first recall classical results on Bloch solutions inside a 2D photonic crystal. This infinite periodic structure is invariant under two fundamental and independent translations vectors $\mathbf{d}$ and Δ, and then the permittivity ε is a periodic function:

$$\text{for all integers } p \text{ and } q, \quad \varepsilon(\mathbf{r} + p\mathbf{d} + q\Delta) = \varepsilon(\mathbf{r}). \tag{1}$$

The Bloch theorem states that each component $u_{\mathbf{k}}(\mathbf{r})$ of an electromagnetic wave propagating inside the crystal can be expressed in the form:

$$u_{\mathbf{k}}(\mathbf{r}) = \exp(i\mathbf{k} \cdot \mathbf{r}) v(\mathbf{r}), \tag{2}$$

where $\mathbf{k}$ is the Bloch wave vector and $v(\mathbf{r})$ is a periodic function:

$$v(\mathbf{r} + p\mathbf{d} + q\Delta) = v(\mathbf{r}), \quad \text{for all integers } p \text{ and } q. \tag{3}$$

For these Bloch modes any translation $p\mathbf{d} + q\Delta$ produces only a phase shift:

$$u_{\mathbf{k}}(\mathbf{r} + p\mathbf{d} + q\Delta) = \exp\left(i\mathbf{k} \cdot (p\mathbf{d} + q\Delta)\right) u_{\mathbf{k}}(\mathbf{r}). \tag{4}$$

In the usual sense of Bloch theorem, the Bloch wave vector $\mathbf{k}$ is real, since one is concerned with bounded solutions. In all this paper we keep this usual definition.

There exists several methods [10–17] to get the solutions $\mathbf{k}(\omega)$, from which the dispersion diagrams can be plotted. In the classical presentation, the solutions are given in the form of a bidimensional diagram where the abscissa represents the edge of the first reduced Brillouin zone. We give in Fig. 1 an example of this diagram in the case of a photonic crystal made of circular rods of radius $\rho = 0.6$, with optical index $v = 2.9$, lying in vacuum. The rods are arranged on a hexagonal lattice with period $d = 4$ (distance between the centers of the rods). The fundamental translations are $\mathbf{d} = d\mathbf{e}_x$ and $\Delta = d(1/2\mathbf{e}_x + \sqrt{3}/2\mathbf{e}_y)$. These parameters are those of a previous work depicted in [18]. Figure 1 has been computed using a plane-wave expansion method [11]. It shows the existence of a gap for $1/\lambda = \omega/(2\pi c)$ between 0.1 and 0.14. All the further examples of this paper will deal with the upper limit of this gap. Indeed, by choosing λ at this limit, we only allow propagation in directions around that given by the X point and its five replicas by hexagonal symmetry.

In order to study the flow of energy inside the crystal, let us recall a fundamental result linking the dispersion relation and the energy

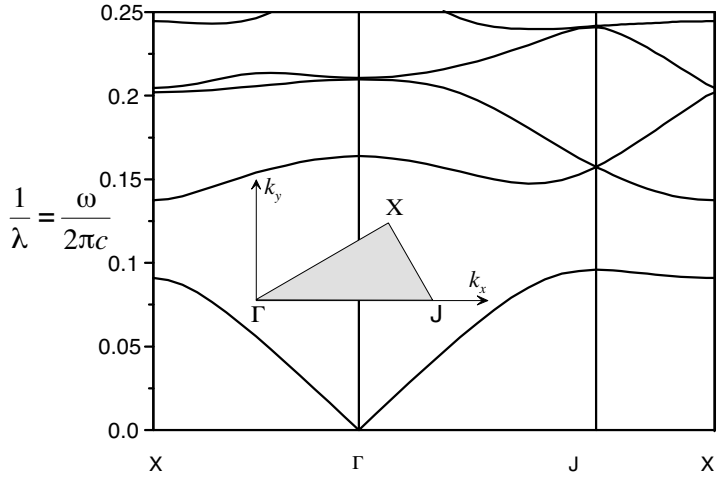

Figure 1. Dispersion diagram for $E\|$ polarization in a 2D crystal with hexagonal lattice. The abscissa represents the Bloch wave vector in the edge of the first reduced Brillouin zone shown in the small insert.

propagation [19]. For a given Bloch wave, the averaged velocity $\mathbf{V}_e$ of the energy flow (the average is taken upon a lattice cell) is equal to the group velocity, i.e.:

$$\mathbf{V}_e = \mathbf{V}_g = \mathbf{grad}_{\mathbf{k}}(\omega) = \frac{\partial \omega}{\partial k_x}\mathbf{e}_x + \frac{\partial \omega}{\partial k_y}\mathbf{e}_y. \tag{5}$$

Thus, the averaged flow of energy is directly linked with the dispersion curve of the Bloch mode $\mathbf{k}(\omega)$. However, the usual representation of the dispersion curve on the edge of the first reduced Brillouin zone do not explicitly show k_x and k_y, and do not contain the information on this group velocity.

This is one of the reasons why we thought that a 3D representation of the same diagram was more convenient for our purpose. Figure 2 shows the same dispersion diagram as Fig. 1, but the Bloch wave vector covers the whole Brillouin zone (in fact (k_x, k_y) belongs to a square region larger than the first reduced Brillouin zone). In this figure, each band is represented by a curved sheet. All the information of Fig. 1 is included in this 3D diagram. In order to obtain the usual 2D view, one should imagine the intersection of the sheets with the vertical walls of a prism whose base is the first Brillouin zone. Furthermore, much more information may be drawn from the 3D diagram. For instance, in an harmonic problem, it is useful to consider the intersection of the sheets with a horizontal plane corresponding to the wavelength of

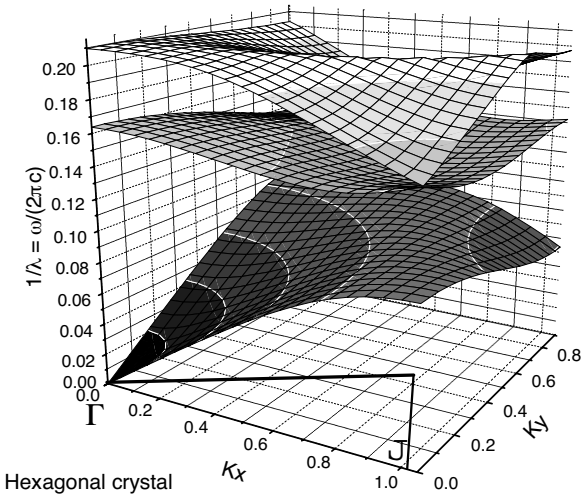

Figure 2. Three-dimensional dispersion diagram. The horizontal plane gives the Bloch wave vector $\mathbf{k}$. The vertical axis gives $1/\lambda$. The triangle corresponding to the first reduced Brillouin zone has been drawn in the (k_x, k_y) plane. The parameters are the same as in Fig. 1.

interest. By this way, we get a curve in the (k_x, k_y) plane that we call constant-frequency dispersion diagram. It can be shown that the direction of the group velocity for a given Bloch mode is the normal to this constant-frequency dispersion diagram. Moreover, the combined use of (5) and Fig. 2 allows one to determine the orientation of this vector, which points towards the increasing values of ω on the sheet of Fig. 2. In a recent paper [20], we give more details on this diagram, as well as its application to the study of ultrarefraction and anomalous refractive properties of photonic crystals. In the present study, we will further make use of the phase velocity $\mathbf{V}_\varphi$ which is proportional to the Bloch wave vector $\mathbf{k}$, and whose modulus is $\omega/||\mathbf{k}||$.

2.2. Crystals with Finite Thickness

Consider now a crystal with finite thickness modeled as a stack of N grids (Fig. 3). The structure is still infinite along the x-direction. Each grid is equivalent to a grating.

First, we suppose that this crystal is illuminated by an incident plane wave:

$$u^{inc}(x, y) = \exp(i\alpha x - i\beta y). \tag{6}$$

As well known, the total field $u_\alpha(x, y)$ is a pseudo-periodic function of

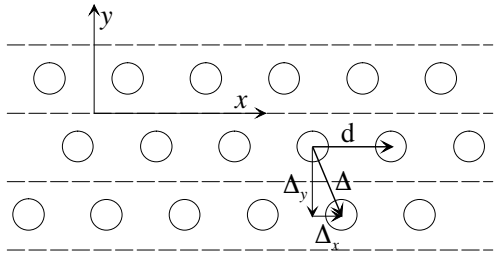

Figure 3. A crystal with finite extent with respect to the y-direction, and made of N gratings (N=3 on this example). The structure is z-independent, and infinite along the x direction. The periodicity along x is d. The distance between two grids is Δ_y. The x-shift between two grids is Δ_x. Thus, the two elementary translations are $\mathbf{d} = d\mathbf{e}_x$ and $\Delta = \Delta_x\mathbf{e}_x - \Delta_y\mathbf{e}_y$. Each grating is characterized by x-periodic electromagnetic parameters, which are not necessarily piecewise constant.

x [21] with pseudo-periodicity coefficient α, i.e.:

$$u_\alpha(x+d,y) = \exp(i\alpha d)u_\alpha(x,y). \tag{7}$$

In this case, it is possible to find a relationship between the allowed Bloch wave vector in the infinite photonic crystal and the pseudo-periodicity coefficient α. A detailed explanation of this link is given in Ref. [20]. Here, we will only give the conclusion and a more intuitive interpretation.

A Bloch mode (in an infinite crystal) is characterized by the fact that the elementary translations $\mathbf{d}$ and Δ (and any of their combinations with integer coefficients) only give rise to phase shifts on the fields (see Eq. (2) and Fig. 3).

As regards the grating case (crystal with finite thickness), the phase shift due to the first translation $\mathbf{d}$ is automatically taken into account by the pseudo-periodicity. The Eqs. (7) and (4) match together when

$$k_x = \alpha. \tag{8}$$

In order to take into account the second translation Δ, let us consider an elementary slice of the crystal (see Fig. 4). We associate with Δ a translation operator T. It transforms any function f as follows:

$$Tf(x,y) = f(x+\Delta_x, y-\Delta_y). \tag{9}$$

Outside the crystal the field can be written as a Rayleigh expansion. Using this basis, the T operator is represented by a $\mathbf{T}$-matrix. The

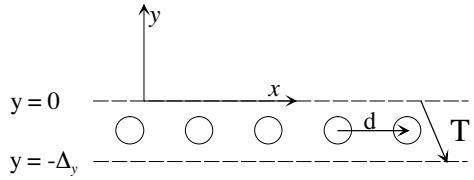

Figure 4. An elementary grating extracted from Fig. 3.

introduction of this matrix is necessary from a numerical point of view. We consider now an eigenvector of the **T**-matrix, with eigenvalue μ:

$$\mathbf{T}u_\mu = \mu u_\mu. \tag{10}$$

When $|\mu| = 1$, Eq. (10) writes:

$$u_\mu(x + \Delta_x, y - \Delta_y) = \exp(i \arg(\mu)) u_\mu(x, y). \tag{11}$$

A comparison between Eqs. (4) and (11) gives:

$$k_y = \frac{k_x \Delta_x - \arg(\mu)}{\Delta_y} \tag{12}$$

Eqs. (8) and (12) point out the link between the grating problem and the Bloch solutions of the infinite structure. Let us emphasize that these results are rigorous, even though they link quantities defined for a finite thickness crystal using a concept (Bloch modes) defined in the case of an infinite crystal. Moreover, Eq. (12) paves the way for getting the dispersion curves of the Bloch problem from the eigenvalues of the **T**-matrix. All the constant-frequency dispersion diagrams presented in the following are obtained by that way.

When $|\mu| \neq 1$, the restriction to the slice $(-\Delta_y \leq y \leq 0)$ of u_μ associated with the eigenvector cannot be a Bloch solution with real vector **k**.

Consequently, for a given value of α, there are two different possibilities for the spectrum of the transfer matrix **T**.

First, if there is no eigenvalue with unit modulus, it seems obvious that we are in a "gap" situation: if the crystal of Fig. 3 is illuminated by an incident plane wave (with a wave vector projection on the x-axis equal to α), the transmitted field through the N gratings tends exponentially toward zero as N increases. This exponential decay is directly related to the modulus of the eigenvalue whose modulus is closest to 1. An example is given in Ref. [20].

Second, if there exists at least one eigenvalue with modulus equal to 1, there is no gap. In other words, there exists at least one Bloch

solution that can propagate in the structure. If the crystal of Fig. 3 is illuminated by a plane wave, the incident field can excite the Bloch solution. But the coupling between the incident field and the Bloch solution also depends on numerous parameters, and in particular on the respective symmetries of these two fields [18, 22–24].

In any case, the field in the grating can never be reduced to a combination of Bloch waves with real Bloch wave vector. The methods that rely upon this assumption can probably give accurate results in some circumstances, but their results should be carefully checked with the help of rigorous methods. The same remark holds for the conclusions directly obtained from dispersion diagrams of Bloch waves. However, as shown in the next sections, these dispersion diagrams are valuable for the prediction and the understanding of the complex properties of photonic crystals.

As well known in grating theory, the **T**-matrix that relates the field above and below a grating suffers from the exponential behavior of its elements. Consequently, the use of the **T**-matrix leads to numerical problems, at least when the structure is composed of several grids. Many other propagation algorithms are more suitable from this point of view [25–29]. As regards our aims, we will make use of the **T**-matrix of one grid only, in such a way that numerical problems are avoided.

Let us come back to the case of the crystal with finite thickness. Now, we suppose that this crystal is illuminated by an arbitrary incident electromagnetic field. For instance, it can be excited by a localized source. Then, the relevant field component can be written as a Fourier integral:

$$u(x,y) = \int_{-\infty}^{+\infty} \hat{u}(\alpha, y) \exp(i\alpha x) d\alpha. \tag{13}$$

By splitting the integration interval $]-\infty, +\infty[$ in subintervals $[(n - \frac{1}{2})\frac{2\pi}{d}, (n + \frac{1}{2})\frac{2\pi}{d}]$, a simple change of variable leads to the other expression:

$$u(x,y) = \int_{-\pi/d}^{\pi/d} u_\alpha(x,y) d\alpha, \tag{14}$$

where the integrand

$$u_\alpha(x,y) = \sum_{m=-\infty}^{-\infty} \hat{u}\left(\alpha + m\frac{2\pi}{d}, y\right) \exp\left(i\left(\alpha + m\frac{2\pi}{d}\right)x\right) \tag{15}$$

is a pseudo-periodic function of x with pseudo-periodicity coefficient α. Consequently, the study of the general field $u(x,y)$ reduces to the study of its pseudo-periodic components $u_\alpha(x,y)$ for all values of α in the first Brillouin zone $[-\pi/d, \pi/d]$ of the x-periodic problem.

3. APPLICATION TO THE DESIGN OF DIRECTIVE SOURCES

In this section, we explain how the tools described in Section 2 can be used to design directive sources. The aim is to realize a device that radiates energy in a very narrow angular range. For that purpose, we want to use only the intrinsic properties of the photonic crystals, and not the properties of a resonant cavity (such as a planar Fabry-Perot cavity). More precisely, our objective is to embed a localized source inside a photonic crystal, and to enforce the radiated field inside a small angular range centered around the normal (i.e., around $\mathbf{e}_y$). Eq. (13) implies that in the homogeneous medium outside the crystal, any radiated field writes as a sum of plane waves. In this sum, the plane waves with significant amplitude should correspond to small values of α (let us assume $\alpha \in [-\alpha_{\max}, \alpha_{\max}]$). Then, from Eq. (8), the allowed Bloch modes of the photonic crystal should lay inside the region $k_x \in [-\alpha_{\max}, \alpha_{\max}]$. In Fig. 5, we represent the dispersion curve of the homogeneous medium outside the crystal. We assume here that this medium is vacuum, and this curve is the circle defined by $k_x^2 + k_y^2 = k_0^2$. The angular range around the vertical direction provides the value of $\alpha_{\max}$. This means that the curves corresponding to the Bloch modes in the constant-frequency dispersion diagram should lay inside the region between the two dashed lines in Fig. 5.

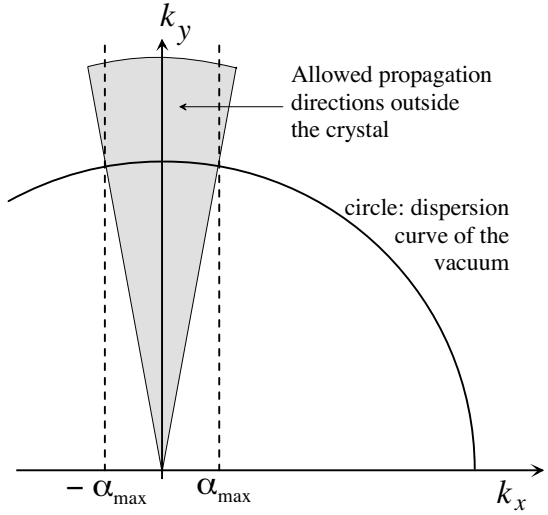

Figure 5. Schematic construction illustrating Eq. (8) and linking the propagation direction outside a grating made with a photonic crystal with the Block wave vector.

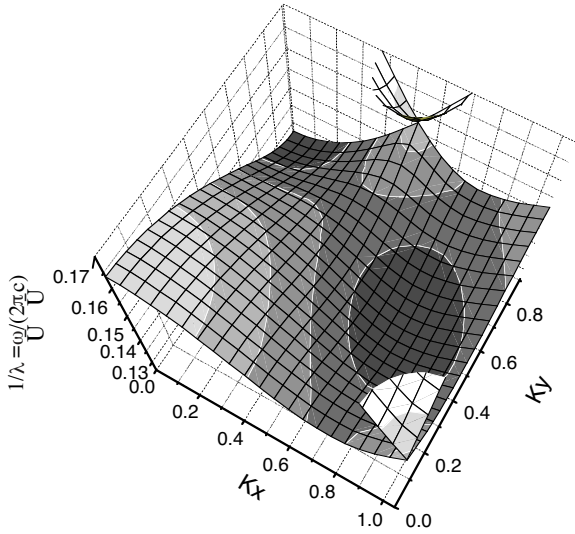

Figure 6. Enlarged view of the central sheet of Fig. 2.

We are now concerned with the following problem: to find a photonic crystal whose constant-frequency dispersion diagram is entirely included in this region. We assume here that the crystal is the same as that depicted in Section 2. Since this diagram is a section by a horizontal plane of the sheets presented in Fig. 2, and because the crystal has an hexagonal symmetry, at the limit of the gap (i.e., $1/\lambda = \omega/(2\pi c)$ close to 0.14) the constant-frequency dispersion diagram reduces to six points (i.e., one point in the first reduced Brillouin zone, the other ones coming from the symmetry). As soon as we move away from the gap by reducing λ, these points become small closed curves.

Fig. 6 presents an enlarged view of the central sheet of Fig. 2. The gap stays behind the main sheet of this figure. In this figure, the six closed curves correspond to the edges of the dark regions (since we represent only a quarter of the Brillouin zone, one should recover the entire diagram using symmetries). It is clear that these six regions are not in the domain which fulfills our requirements (i.e., only in a small band $k_x \in [-\alpha_{\max}, \alpha_{\max}]$). The dark region in the top of the figure lay indeed in the required domain (and its symmetric with respect to the k_x axis also), but the four other regions deduced by hexagonal symmetry get large values of k_x (it is for example the case of the right most dark region).

One way to overcome this problem is to break the symmetry. We

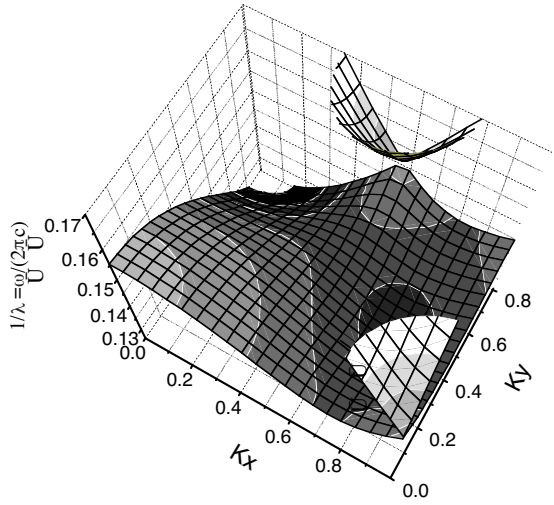

Figure 7. The same as Fig. 6, but for the expanded crystal.

have chosen to expand the cell of the crystal in the y direction: the vertical spacing between two grids is enlarged from $\sqrt{3}d/2 \approx 3.46$ to 3.9. All the rods keep the same parameters, and in particular their radius is always $\rho = 0.6$. Fig. 7 shows the same 3D dispersion diagram as Fig. 6, but for this expanded crystal. Clearly, this diagram does not present any more the invariance under 60 degrees rotation property. Moreover, it emerges that it is possible to choose a value of λ such that the constant dispersion diagram stays in the required band. For instance, at the wavelength $\lambda = 7.93$ corresponding to the horizontal plane at the bottom of Fig. 7, the constant-frequency dispersion diagram reduces to a small curve. In Fig. 7, this curve is the limit between the dark and white regions in the left-hand upper corner. It is represented in the (k_x, k_y) plane in Fig. 8.

At this stage, any source at $\lambda = 7.93$, embedded in a slice of this expanded photonic crystal will radiate a plane-wave packet:

$$u(x,y) = \int_{-\infty}^{+\infty} A(\alpha) \exp(i\alpha x \pm i\beta(\alpha) y) d\alpha, \tag{16}$$

with $\beta^2 = k_0^2 - \alpha^2$ and $\arg(\beta) \in \{0, \pi/2\}$. The sign in the exponential depends on the region where the field is radiated (above or below the crystal). In this packet, the plane waves with significant amplitude $A(\alpha)$ correspond to small values of α. Note that we neglect the evanescent modes (those for which $|\mu| \neq 1$ in section 2.2. In other

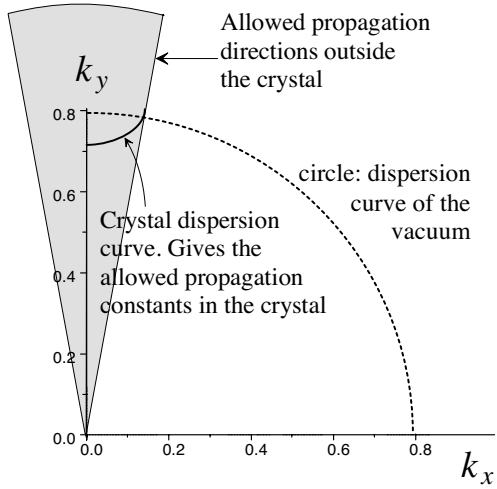

Figure 8. Constant-frequency dispersion diagram of the expanded crystal for $\lambda = 7.93$.

words, the source should be surrounded by a sufficient thickness of photonic crystal.

Because of the up-down symmetry, the radiation occurs for both $+\mathbf{e}_y$ and $-\mathbf{e}_y$ directions. One way to eliminate one of these directions is to use a ground plane (or a mirror). Here, another solution has been chosen. The initial hexagonal crystal is used as a mirror, since the wavelength $\lambda = 7.93$ is inside a gap of this crystal.

It is worth noticing that all the previous considerations deal with a crystal with infinite extension along the x-axis. We now model a crystal with finite extension along this direction. Consequently, one should expect some discrepancies with the theoretical conjecture and the numerical study will allow us to determine the influence of the lateral size of the structure on the expected phenomenon. We use a modal theory based on scattering matrices, the fields being expressed as Fourier Bessel series [30, 18]. This method rigorously solves the problem of scattering from a finite set of parallel rods.

The structure is shown in Fig. 9. In our 2D formalism, we can use an arbitrary incident field. Here, the excitation is provided by an infinitely thin wire source located in the expanded crystal at a point $\mathbf{r}_0$ with coordinates $x_0 = 0$, $y_0 = 34$. Consequently, our incident field generates an $E\|$ polarized field and is given by

$$u^{inc}(\mathbf{r}) = H_0^{(1)}(k_0||\mathbf{r} - \mathbf{r}_0||), \tag{17}$$

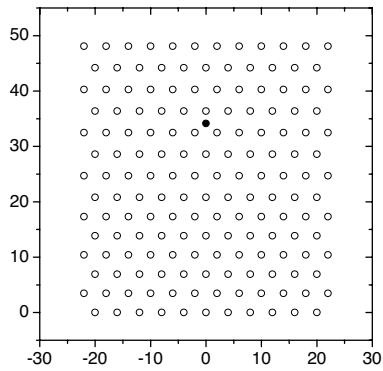

Figure 9. Superposition of a hexagonal photonic crystal ($0 < y < 20.8$) and of a vertically expanded crystal ($20.8 < y < 48.1$). The wire source located at $x_0 = 0$, $y_0 = 34$ is represented by a black point.

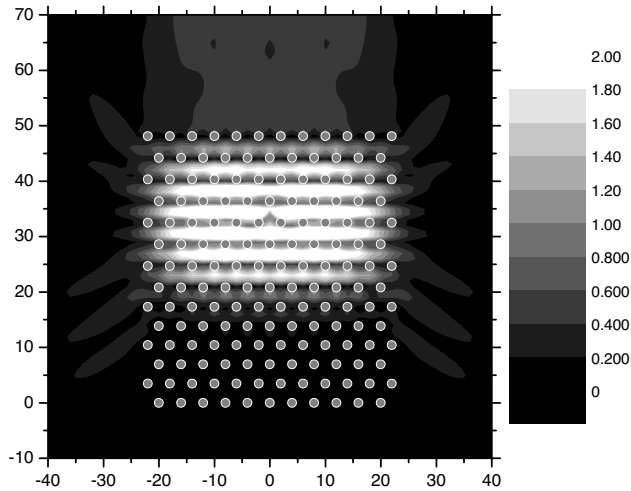

Figure 10. Total field modulus radiated by the structure of Fig. 9 excited by the wire source at $\lambda = 7.93$.

the amplitude of the Hankel function being taken equal to unity for simplicity.

Fig. 10 shows the map of the total field modulus, and Fig. 11 the energy emission diagram in arbitrary units. The overall appearance of the field map can be explained using the Bloch modes. Indeed, if we neglect the evanescent modes, the propagating Bloch modes are governed by the constant-frequency dispersion diagram shown in Fig. 8

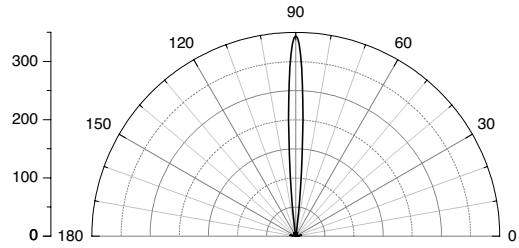

Figure 11. Polar emission diagram for the structure of Fig. 9 excited by the wire source at $\lambda = 7.93$.

(which must be completed by symmetry). Since the Bloch wave vector has a small k_x component and a larger k_y component, and according to Eq. (2), the average field variation along the x-axis is slow, and the average field variation along the y-axis is much faster. This property is clearly shown by Fig. 10. Another interesting feature can be explained using the constant-frequency dispersion diagram. We know that the average energy flow of the Bloch mode points toward the normal to the constant-frequency dispersion diagram. In that case, this diagram is a small closed curve (Fig. 8), and thus the energy flows in all directions. The consequences are that the energy radiated by the wire flows in the whole expanded crystal, and that the phenomenon is not sensitive to the location of the wire. Fig. 11 shows that the field is radiated in a narrow angular range. The half-power beamwidth is equal to $\pm 4.0^\circ$ with respect to the normal. Note that the half-power beamwidth of the field radiated by a screen pierced by an aperture having a width w of 45 (the transverse dimension of our structure), illuminated by a field with constant amplitude and phase would be $\pm 0.443\lambda/w = \pm 4.5^\circ$. The main interesting feature of the structure is to generate a field with slow transverse variation using almost any excitation (in this case, a simple wire).

In order to reduce the half-power beamwidth, it appears that the lateral size of the structure must be widened. Fig. 12 is equivalent to Fig. 10, but the lateral size of the structure is $w = 76$. Now, the field shows important transverse variations inside the structure, and we can observe two regions with high field amplitude. Consequently, the radiated energy pattern shown in Fig. 13 exhibits secondary lobes.

The spatial variations of the field along the x-axis in Fig. 12 can be reduced if the wavelength is increased in order to get closer to the band-gap edge. Indeed, the constant-frequency dispersion diagram will become a smaller closed curve, and thus the allowed k_x components of the Bloch wave vector will become smaller too. Fig. 14 illustrates

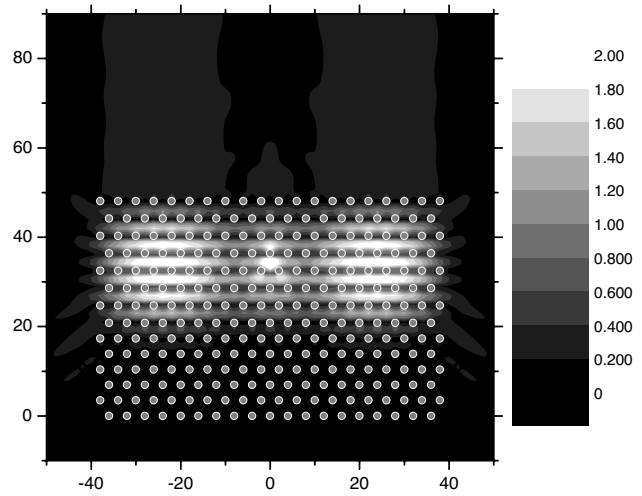

Figure 12. Total field modulus radiated by a widened structure, excited by the wire source at $\lambda = 7.93$.

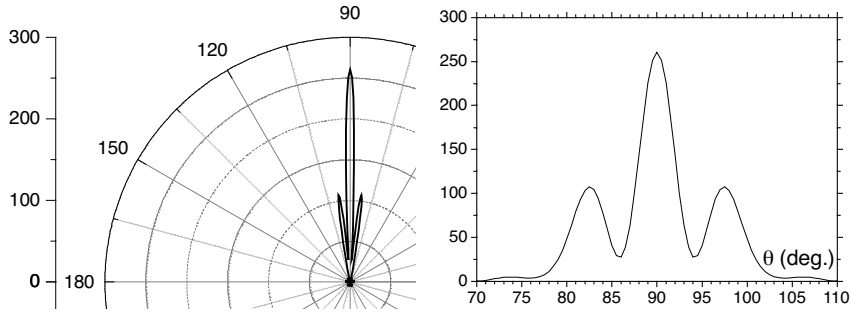

Figure 13. Left: polar emission diagram for the structure of Fig. 12. Right: the same in cartesian coordinate.

this behavior. For a wavelength equal to 7.96, the spatial variations of the field along the x-axis are smooth and the radiated energy pattern shown in Fig. 15 presents one principal lobe only. The half-power beamwidth is equal to $\pm 2.8°$ apart from the normal and is very close to the half-power beamwidth $\pm 2.6°$ of the field radiated by an aperture in a screen with a width w of 76.

Narrower radiation patterns can be obtained by increasing the lateral size of the structure. But the wavelength should get closer and closer to the band-gap edge and the range of possible wavelengths would be reduced.

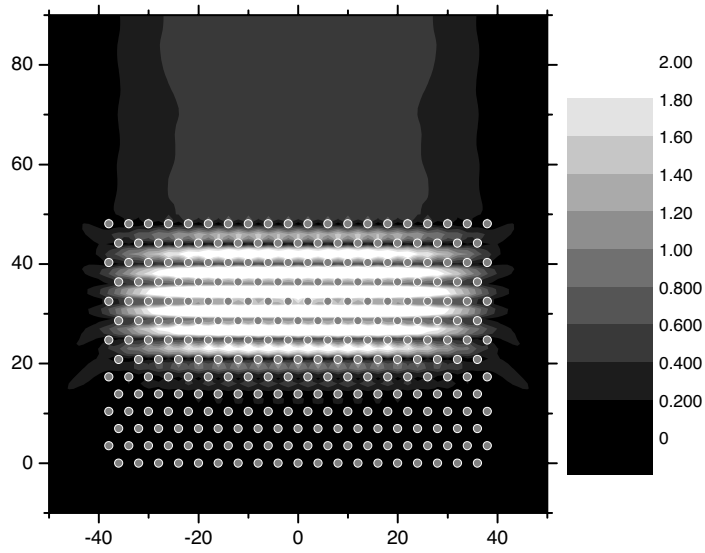

Figure 14. Total field modulus radiated by the same structure as in Fig. 12, but now excited by the wire source at $\lambda = 7.96$.

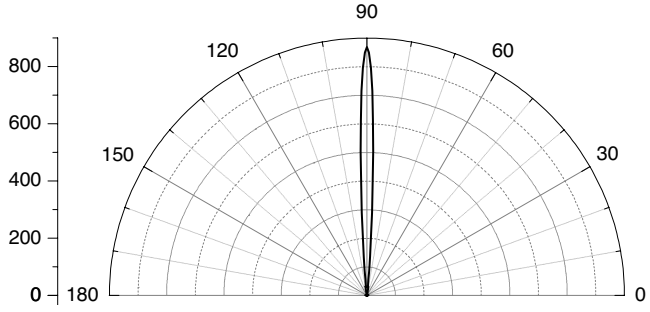

Figure 15. Polar emission diagram for the structure of Fig. 14.

4. OFF-AXIS RADIATION DEVICE

Our approach allows us to design an emitting device radiating a narrow beam in any direction (and not necessarily toward the normal). To this end, we need to rotate the constant-frequency dispersion diagram. This is done by rotating the expanded crystal.

In the previous section, we have mentioned two ways for eliminating the down propagating field (photonic crystal used in the gap

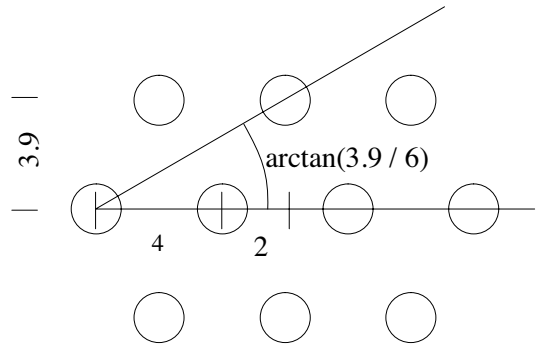

Figure 16. Rotation of the expanded crystal.

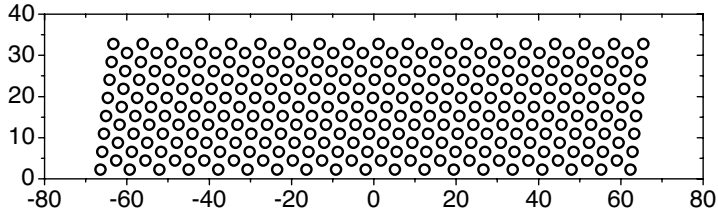

Figure 17. Rotated expanded crystal laying above a ground plane.

or ground plane). In this section we have chosen to illustrate the second possibility. Note that this model (the ground plane) is more pertinent in the microwaves range. The ground plane is supposed to be an infinitely conducting plane interface of infinite extension, placed in the plane $y = 0$.

We have chosen to rotate the expanded crystal with an angle of $33^\circ \approx \arctan(3.9/6)$. This choice allows us to obtain a lower row of rods parallel to the ground plane (see Figs. 16 and 17).

Fig. 18 shows the field map when this crystal is excited by a wire source at $\lambda = 8.01$ located at $x_0 = 0$ and $y_0 = 4$. The wavelength is chosen in such a way that the field flows in the entire crystal. In that case the transverse variations of the field are smooth in a direction orthogonal to the desired emitting direction. The Bloch mode propagating inside the crystal enforces an appropriate field phase on the upper boundary of the crystal. This phase is appropriate since it is close to that of a plane wave propagating at 33° with respect to the normal. This example also shows that the location of the wire source is not critical. We see that the field is not particularly large near the source, and the largest values are located in the middle of the crystal.

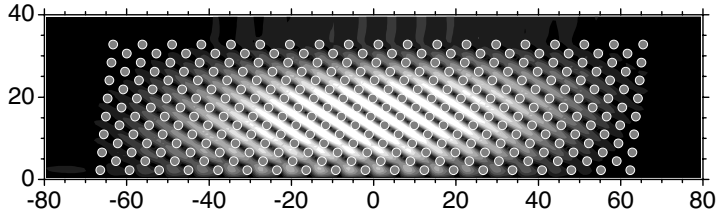

Figure 18. Total field modulus radiated by the structure of Fig. 17, excited by a wire source at $\lambda = 8.01$, located at $x_0 = 0$ and $y_0 = 4$.

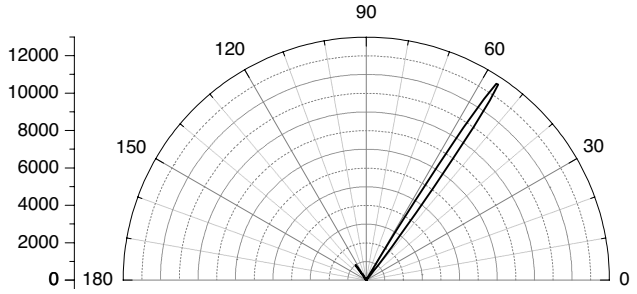

Figure 19. Polar emission diagram for the structure of Fig. 18.

This property is useful, since it allows one to choose the position of the source in order to obtain a convenient input impedance.

Fig. 19 shows the polar emission diagram for the same structure with the same parameters. As expected, the principal lobe is tilted by an angle of 33° from the normal. A small part of the energy radiates in the symmetric direction. Assuming again that the outgoing wave has a constant amplitude on the crystal, the half-power beamwidth should be equal to $\pm 0.443\lambda/(w \cos 33°) = \pm 1.9°$, where $w = 130$ is the lateral size of the crystal. The actual half-power beamwidth obtained on the emission diagram is $\pm 2.1°$. This agreement shows the relevance of our approach.

5. CONCLUSION

We have developed a synthetic approach using the dispersion relations of the Bloch modes inside an infinite photonic crystal, which allowed us to anticipate the behavior and the radiative properties of a finite-size photonic crystal. The main result is that if the constant-frequency dispersion diagram is included in a small band of the Brillouin zone

corresponding to a small range of the lateral component of the Bloch wave vector, and if the structure has a sufficiently large lateral size, then the emission occurs in a narrow lobe. All the steps yielding to the design of a directive source using a dielectric photonic crystal have been given.

This approach is based on the specific properties of the photonic crystals, and not on resonant properties of a cavity, such as for instance a Perot-Fabry cavity, or resonances induced by defects in the crystal. These specific properties are obtained near the band-gap edge. We have shown that in order to get radiation in a single direction, it can be useful to break the symmetries of the photonic crystal. This is done in our examples by expanding the lattice in a convenient direction. Moreover, we have shown that it is possible to choose arbitrarily the direction of the major emission lobe.

This study can be generalized to the case of metallic photonic crystals, as well as to the case of three-dimensional photonic crystals. The work is in progress in that direction and it will be reported soon.

REFERENCES

1. Yang, H. Y. D., N. G. Alexopoulos, and E. Yablonovitch, "Photonic band-gap materials for high-gain printed circuit antennas," *IEEE Trans. on Antennas and Propagat.*, Vol. 45, 185–187, 1997.
2. Sigalas, M. M., R. Biswas, Q. Li, D. Crouch, W. Leung, R. Jacobs-Woodbury, B. Lough, S. Nielsen, S. McCalmont, G. Tuttle, and K. M. Ho, "Dipole antennas on photonic band-gap crystals-Experiment and simulation," *Microwave and Optical Technology Letters*, Vol. 15, 153–158, 1997.
3. Leung, W. Y., R. Biswas, S. D. Cheng, M. M. Sigalas, J. S. McCalmont, G. Tuttle, and K. M. Ho, "Slot antennas on photonic band gap crystals," *IEEE Trans. on Antennas and Propagat.*, Vol. 45, 1569–1570, 1997.
4. Smith, G. S., M. P. Kesler, and J. G. Maloney, "Dipole antennas used with all-dielectric, woodpile photonic-bandgap reflectors: gain, field pattern, and input impedance," *Microwave and Optical Technology Letters*, Vol. 21, 191–196, 1999.
5. Sievenpiper, D., L. Zhang, R. F. Jimenez Broas, N. G. Alexopoulos, and E. Yablonovitch, "High-impedance electromagnetic surfaces with a forbidden frequency band," *IEEE Transactions on Microwave Theory and Techniques*, Vol. 47, 2059–2074, 1999.
6. Gonzalo, R., P. de Maagt, and M. Sorolla, "Enhanced patch-

antenna performance by suppressing surface waves using photonic-bandgap substrates," *IEEE Transactions on Microwave Theory and Techniques*, Vol. 47, 2131–2138, 1999.

7. Gonzalo, R., B. Martinez, P. de Maagt, and M. Sorolla, "Improved patch-antenna performance by using photonic-bandgap substrates," *Microwave and Optical Technology Letters*, Vol. 24, 213–215, 2000.
8. Thèvenot, M., C. Cheype, A. Reinex, and B. Jecko, "Directive photonic-bandgap antennas," *IEEE Transactions on Microwave Theory and Techniques*, Vol. 47, 2115–2122, 1999.
9. Temelkuran, B., M. Bayindir, E. Ozbay, R. Biswas, M. M. Sigalas, G. Tuttle, and K. M. Ho, "Photonic crystal-based resonant antenna with a very high directivity," *Journal of Applied Physics*, Vol. 87, 603–605, 2000.
10. Ho, K. M., C. T. Chan, and C. M. Soukoulis, "Existence of photonic gap in periodic dielectric structures," *Phys. Rev. Lett.*, Vol. 65, 3152–3155, 1990.
11. Plihal, M. and A. A. Maradudin, "Photonic band structure of two-dimensional systems: the triangular lattice," *Phys. Rev. B*, Vol. 44, 8565–8571, 1991.
12. Sözüer, H. S., J. W. Haus, and R. Inguva, "Photonic bands: convergence problems with the plane-wave method," *Phys. Rev. B*, Vol. 45, 13962–13972, 1992.
13. Joannopoulos, J., R. Meade, and J. Winn, *Photonic Crystals*, Princeton University Press, 1995.
14. Meade, R. D., A. M. Rappe, K. D. Brommer, J. D. Joannopoulos, and O. L. Alerhand, "Accurate theoretical analysis of photonic band-gap materials," *Phys. Rev. B*, Vol. 48, 8434–8437, 1993. See also the erratum in *Phys. Rev. B*, Vol. 55, 15942, 1997.
15. Moroz, A. and C. Sommers, "Photonic band gaps of three-dimensional face-centered cubic lattices," *J. Phys.: Condens. Matter*, Vol. 11, 997–1008, 1999.
16. Botten, L. C., N. A. Nicorovici, R. C. McPhedran, C. M. de Sterke, and A. A. Asatryan, "Photonic band structure calculations using scattering matrices," *Phys. Rev. E*, Vol. 64, 2001.
17. Botten, L. C., R. C. McPhedran, N. A. Nicorovici, A. A. Asatryan, C. M. de Sterke, P. A. Robinson, K. Busch, G. H. Smith, and T. N. Langtry, "Rayleigh multipole methods for photonic crystal calculations," *PIER*, Special Issue on electromagnetic applications of PBG materials and structures, Itoh, T. and A. Priou (Eds.).
18. Tayeb, G. and D. Maystre, "Rigorous theoretical study of finite

size two-dimensional photonic crystals doped by microcavities," *J. Opt. Soc. Am. A*, Vol. 14, 3323–3332, 1997.

19. Yeh, P., "Electromagnetic propagation in birefringent layered media," *J. Opt. Soc. Am.*, Vol. 69, 742–756, 1979.
20. Gralak, B., S. Enoch, and G. Tayeb, "Anomalous refractive properties of photonic crystals," *J. Opt. Soc. Am. A,* Vol. 17, 1012–1020, 2000.
21. Petit, R. (Ed.), *Electromagnetic Theory of Gratings*, Springer-Verlag, 1980.
22. Villeneuve, P., S. Fan, and J. D. Joannopoulos, "Microcavities in photonic crystals: mode symmetry, tunability, and coupling efficiency," *Phys. Rev. B*, Vol. 54, 7837–7842, 1996.
23. Sentenac, A., J. J. Greffet, and F. Pincemin, "Structure of the electromagnetic field in a slab of photonic crystal," *J. Opt. Soc. Am. B*, Vol. 14, 339–347, 1997.
24. Yuan, Z., J. W. Haus, and K. Sakoda, "Eigenmode symmetry for simple cubic lattices and the transmission spectra," *Optics Express*, Vol. 3, 19–27, 1998.
25. Hall, R. C., R. Mittra, and K. M. Mitzner, "Analysis of multilayered periodic structures using generalized scattering matrix theory," *IEEE Trans. Ant. Prop.*, Vol. 36, 511–517, 1988.
26. Nevière, M. and F. Montiel, "Deep gratings: a combination of the differential theory and the multiple reflection series," *Optics Comm.*, Vol. 108, 1–7, 1994.
27. Montiel, F. and M. Nevière, "Differential theory of gratings: extension to deep gratings of arbitrary profile and permittivity through the R-matrix propagation algorithm," *J. Opt. Soc. Am. A*, Vol. 11, 3241–3250, 1994.
28. Li, L., "Bremmer series, *R*-matrix propagation algorithm, and numerical modeling of diffraction gratings," *J. Opt. Soc. Am. A*, Vol. 11, 2829–2836, 1994.
29. Li, L., "Formulation and comparison of two recursive matrix algorithms for modeling layered diffraction gratings," *J. Opt. Soc. Am. A*, Vol. 13, 1024–1035, 1996.
30. Felbacq, D., G. Tayeb, and D. Maystre, "Scattering by a random set of parallel cylinders," *J. Opt. Soc. Am. A*, Vol. 11, 2526–2538, 1994.